Growing-In of Optical Coherence in the FMO Antenna Complexes[§]

V. I. Prokhorenko,*[,†] A. R. Holzwarth,[†] F. R. Nowak,[‡] and T. J. Aartsma[‡]

Max-Planck Institut für Strahlenchemie, Stiftstr. 34-36, D-45470 Mülheim a.d. Ruhr, Germany and Department of Biophysics, Huygens Laboratory, Leiden University, P.O. Box 9504, 2300 RA Leiden, The Netherlands

Received: March 13, 2002; In Final Form: July 9, 2002

We report on the novel effect of the growing-in of optical coherence in the FMO antenna complexes. The rise of coherence, monitored by femtosecond two-pulse photon echo spectroscopy at 1.27 K, occurs within a characteristic time of 150−250 fs after impulsive excitation at the red edge of the absorption spectrum and is accompanied by strong and long-lasting oscillations. We show that this effect cannot be explained in the framework of present theories for the photon echo formation. To account for the observations, we take into consideration a finite system-bath interaction time and develop the theory beyond the Markov limit. We show that the coherence does not follow the impulsive excitation promptly, instead its time development is delayed. General expressions are obtained for the nonlinear polarization, which can also be applied for analysis of other time-resolved experiments (three-pulse photon echoes, transient grating, transient absorption etc.). Model calculations fully support our experimental observations.

I. Introduction

The study of the pigment−protein interaction dynamics plays an important role for understanding the primary functions in photosynthesis such as energy transfer and primary charge separation. The simplest and most straightforward manner to characterize these interactions would be coherent spectroscopy of a single pigment molecule, immersed into a well-defined protein environment. Unfortunately, such an ideal object is not readily available. However, a situation quite close to that is realized in the bacteriochlorophyll (BChl) *a*-protein Fenna-Matthews-Olson complexes (FMO) of the green sulfur bacteria *Chlorobium tepidum* and *Prosthecochloris aestuarii*. Their spatial structure has been determined with near-atomic resolution.[1,2] Both contain three identical subunits, related by a 3-fold axis of symmetry. Each subunit comprises seven BChl *a* molecules, embedded into a protein pocket. According to exciton simulations of steady-state optical spectra (absorption, circular dichroism, linear dichroism, and triplet-minus-singlet absorption[3]), pigment #3 (numbering according to Fenna and Matthews[1]) can be considered as an essentially isolated molecule which contributes 80−90% to the lowest exciton state at ∼825 nm.[4] This BChl *a* molecule determines mainly the well-resolved long-wavelength peak in the absorption (Figure 1). However, for the excitonically coupled system, it is essential to consider also the possible contribution of double-excited states (the so-called bi-excitonic states). This contribution appears e.g., in pump−probe experiments as an excited-state absorption (ESA). For the FMO complexes the measurements and exciton calculations[5−7] show however that the ESA does not contribute significantly at the red edge of the absorption (∼825 nm). Thus we can conclude, that in the 825 nm region the absorption of the FMO antenna complexes is determined mostly by a *single* BChl-molecule (#3) interacting with the protein.

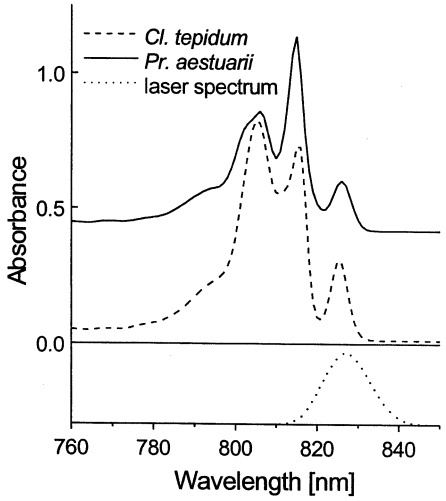

Figure 1. Absorption spectra of the two FMO complexes at 6 K. For clarity of representation, an offset of 0.4 was added to the *Pr. aestuarii* spectrum. The laser spectrum (as used for PE measurements) measured at 827 nm is shown at the bottom.

We present here a photon echo (PE) study of two different FMO complexes, performed at low temperature (1.27 K) using the simple two-pulse (2PE) technique. We focus attention on the unusual behavior of the 2PE-signals at the red edge of absorption, where we observe a delayed growing-in of coherence for both FMO complexes, accompanied by strong and underdamped oscillations.

The present paper is organized as follows. In section III, we show the main features of the time evolution of coherence, monitored by means of 2PE, discuss the nature of the observed oscillations and consider possible effects which can cause a growth of coherence. We analyze this effect and show that the growth of coherence cannot be explained in the framework of existing theories of photon echo formation. In section IV, we

* To whom correspondence should be addressed. E-mail: prokh@mpi-muelheim.mpg.de. Fax (+49)208-306-3951.
[†] Max-Planck Institut für Strahlenchemie.
[‡] Department of Biophysics, Huygens Laboratory, Leiden University.
[§] A preliminary account of this work has been given at the XIIth International Conference on Ultrafast Phenomena, Charleston, S.C. (2000). In *Ultrafast Phenomena XII*, edited by T. Elsaesser, S. Mukamel, M. M. Murnane, and N. F. Scherer, Springer, 2000.

10.1021/jp025758e CCC: $22.00
Published on Web 08/27/2002

explain this effect using a density matrix formalism beyond the Markov limit and show that due to a finite time of system-bath interaction the development of coherence is delayed. This novel effect is then tested by comparison of theoretically calculated induced polarization for both Markov and non-Markov approximations. Finally, we develop the theory of PE formation beyond the Markov limit, apply it to calculations of the 2PE-signal using available experimental data, and compare it with the measurements.

II. Experimental Section

Sample Preparation. FMO-complexes from *Pr. aestuarii* and *Cl. tepidum* were isolated and purified as described by Francke and Amesz.[8] They were dissolved in 50 mM Tris/HCl and 200 mM sodium chloride (pH 8.3). The samples were diluted 2-fold with glycerol to obtain a high optical quality at liquid helium temperatures, and the optical density was adjusted to ≤ 1 in a 0.5 mm cell of 15 μL volume. The filled cell was slowly cooled to 4.2 K by immersing it in a bath cryostat with liquid helium. Figure 1 shows the absorption spectra, measured in situ at 6 K.

2PE Setup. The experiments have been carried out using an optical setup as described in detail elsewhere.[9] Briefly, the laser pulses at a repetition rate of 80 kHz from the tunable Ti:Sapphire laser, with duration of 80−90 fs and spectral width of 11 nm (see Figure 1), were split into two collinear beams and focused by a lens ($f = 120$ cm) into the sample, which was immersed in a pumped helium-bath cryostat (model B29, Institute of Physics, Kiev, Ukraine). The measurements were carried out at 1.27 K. The 2PE signal was monitored at different excitation wavelengths in the $2k_1$-k_2 direction by delaying the second beam in several delay scan ranges of 2.5, 6, 12.5, and 300 ps with delay steps of 6.7, 13.4, and 600 fs, respectively. The density of the excitation energy was about 5×10^{12} photon/cm^2/pulse. Under these conditions, the estimated average number of excitations per FMO complex was ~0.005/pulse which excludes any appreciable creation of bi-excitonic states, and also the accumulation of triplet states of BChl *a* is negligibly small. We estimated a local heating in the sample under these excitation conditions using the Poisson equation for the stationary heat diffusion. The increase of the local temperature in the focus of the laser beam was calculated to be ~0.005 K.

Data Treatment. Analysis of the measured 2PE-signals was performed independently for each wavelength, or simultaneously for a set of traces (window 815−832 nm) using global analysis with a deconvolution procedure in a multiexponential fashion

$$S_{\mathrm{PE}}(\tau, \lambda) = \sum_i A_i(\lambda) \int_0^\infty CCF^{(3)}(\tau - t) e^{-t/\tau_i} dt \qquad (1)$$

where S_{PE} denotes the measured signal, τ is the delay time between laser pulses, A_i is the amplitude of the i^{th} decay component with characteristic dephasing constant[10] τ_i, λ is wavelength, and $CCF^{(3)}$ is the third-order cross-correlation function of the laser pulses

$$CCF^{(3)}(\tau) \propto \int_{-\infty}^{\infty} I^2(t) I(t + \tau) dt \qquad (2)$$

where $I(t)$ is the laser pulse intensity envelope. This situation differs from pump−probe (or time-resolved fluorescence) experiments where the exponentials are convoluted with the second-order cross-correlation function, because the photon echo is a *third-order* nonlinear effect (for details see Appendix A in ref 11). In the present work, we were not able to measure the third-order *CCF* directly. Instead the second-order $CCF^{(2)}$ was recorded at each wavelength. However, by assumption that the laser pulses obey a Gaussian shape (typical for self-mode-locked Ti:Sapphire lasers), the third-order $CCF^{(3)}$ will be related to the measured second-order $CCF^{(2)}$ as

$$CCF^{(3)}(\tau) \propto [CCF^{(2)}(\tau)]^{1.5} \qquad (3)$$

which we used for the deconvolution procedure. The global data analysis resulting in the decay-associated spectra (DAS) was performed by assuming that the decay times were constant in the analyzed wavelength range. The DAS were absorption corrected according to the procedure described in.[11]

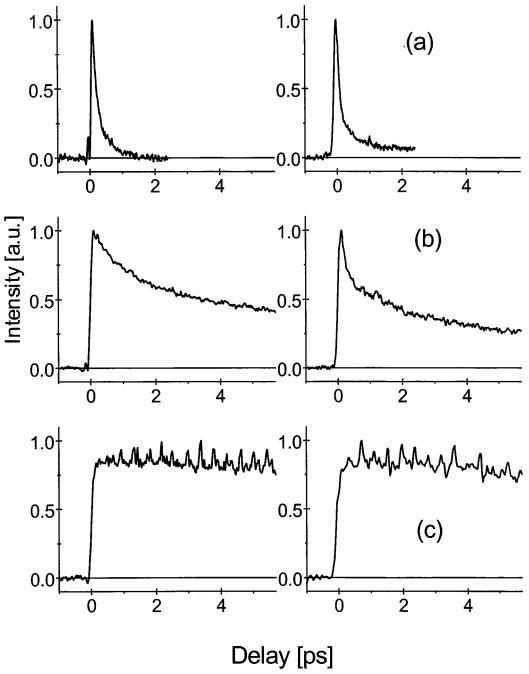

Figure 2. Photon echo traces, measured at 800 nm (a), 815 nm (b), and 825 nm (c). Left − FMO from *Cl. tepidum*, right − FMO from *Pr. aestuarii*.

III. Results and Discussion

Figure 2 demonstrates the recorded 2PE traces from both FMOs for excitation at different wavelengths. As can be seen, for excitation at the "blue" side of the absorption the 2PE signal displays a fast dephasing within a time of ~150−200 fs (Figure 2a), which is mainly due to the fast energy transfer within the manifold of exciton states, occurring within 170−500 fs at low temperatures.[6,12,13] For excitation at the "red" edge of absorption where the lowest exciton transition is located, no uphill energy transfer is possible at 1.27 K, and dephasing at early times can occur in principle only due to the interaction of the excited molecule (BChl #3) with the protein. This would leads to the well-known prompt decay of coherence immediately after excitation. In vast contrast to that expectation, we observe however a growing-in of the 2PE-signal, accompanied by highly reproducible strong oscillations (Figure 2c). Their relative amplitude, plotted in Figure 3, increases by tuning of the excitation wavelength further to the red, reaching ~40% at 832 nm. Monitoring over a large delay window (Figure 4) shows that these oscillations persist more or less un-damped over times up to 300 ps. The inset in Figure 4 demonstrates three different 2PE-scans, performed around 100 ps in a delay window of 6 ps with high resolution. As can be seen, apart from a noise component, all of these traces contain characteristic oscillations with the same frequencies. The Fourier transform of the

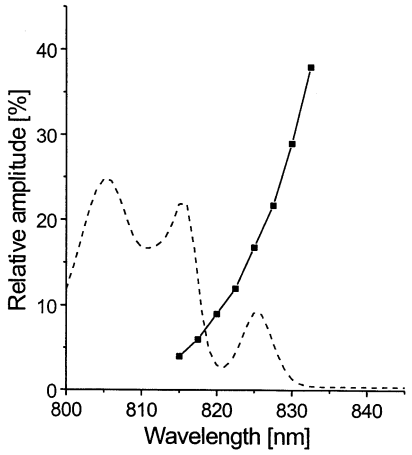

Figure 3. Relative amplitude of oscillations in 2PE traces for FMO from *Cl. tepidum* at different wavelengths. For better comparison, the absorption spectrum is also plotted (dashed line).

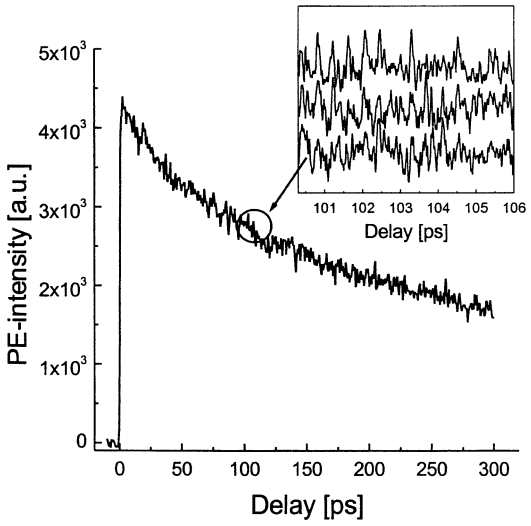

Figure 4. 2PE signal from FMO of *Cl. tepidum* at 830 nm. The trace was measured with a delay step of 0.6 ps. The inset shows three different scans taken around 100 ps delay with step size of 6.7 fs.

residuals, performed in a 5 ps window starting from zero delay, reveals the presence of at least 3 equally spaced components with frequencies of 80, 150−160, and 240 cm^{-1} for both FMO complexes (Figure 5). The highest frequency modes could not be fully resolved due to the relatively narrow laser excitation spectrum (∼160 cm^{-1} of fwhm).

These oscillations could originate from the quantum beating between the lowest exciton state (825 nm) and the next higher state(s) located at 815 nm because by excitation with ∼11 nm spectral width some part of the 815 nm transitions still has overlap with the laser spectrum. Such oscillations with a frequency of 150 cm^{-1} (actually close to the second component in the Fourier spectra of Figure 5) were observed in pump−probe experiments with ∼9 nm bandwidth of the laser spectrum.[14] However, in that study it was also demonstrated that they are fully damped within ∼1 ps, and by tuning to the red edge of the absorption their relative amplitude decreases rapidly. In contrast, in the 2PE-signal the relative amplitude of oscillations *increases* strongly by tuning the excitation wavelength to the red edge (Figure 3), and they show no significant damping within at least 100 ps (Figure 4). Thus, we can conclude that the observed oscillations in the 2PE-signals must originate from vibrational states of BChl *a* in the ground state. Vibrational

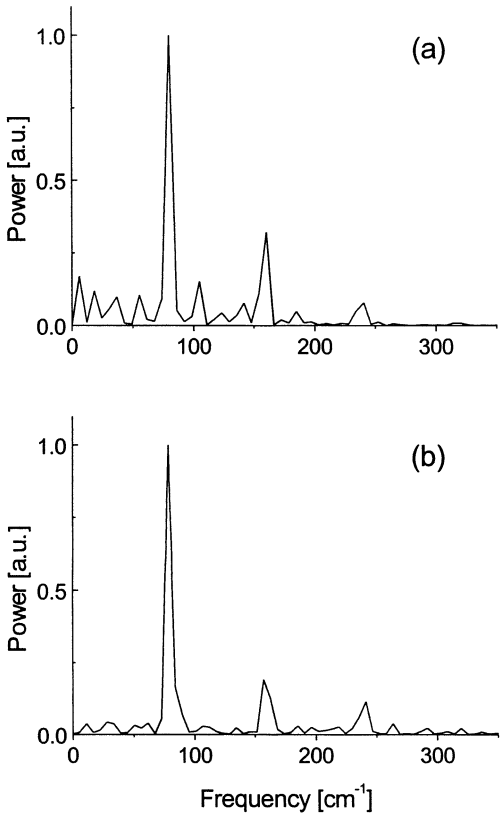

Figure 5. Fourier spectra of the oscillations in the 2PE traces from FMO of *Pr. aestuarii* (a) and *Cl. tepidum* (b). Delay window 5 ps.

transitions with frequencies close to the observed oscillations were resolved in the low-temperature site-selective fluorescence spectrum (70, 173, and 237 cm^{-1}, Table 1 in [15]), which reflects properly the homogeneous absorption spectrum.[16] However, these modes are significantly narrowed in the Fourier-spectrum of the 2PE-traces as compared to the fluorescence spectrum. Note that the appearance of vibrational transitions in the photon echo signals was earlier demonstrated in the APE-experiments.[17−19]

The time evolution of coherence at the red edge of the absorption can be characterized by two slow decay components in the picosecond time range, and a *rise component* of ∼240 fs (for FMO *Cl. tepidum* the 2PE grows within a time of ∼150 fs). Figure 6 shows the 2PE signals, recorded at 825 nm, and the fitted curves (a single trace fit). By tuning the excitation wavelength it was found that the maximum of the growth component amplitude corresponds to the 825-nm red absorption peak for both FMOs. Figure 7 shows the decay-associated spectra (DAS) of the 2PE traces, recorded in the window of 815−832 nm for FMO from *Cl. tepidum*. It should be pointed out that the 2PE traces, measured at the red edge of absorption, could in no way be fitted reasonably without the rise component. Essentially, the same observations were made in accumulated photon echo (APE) investigations, performed in a completely different setup.[20] However, the time resolution of the latter experiments (∼1 ps) was not quite sufficient for an unequivocal assignment.

The presence of the rise component in the photon echo signal indicates that the coherence is growing after excitation, i.e., the optically excited molecule develops the coherent state not promptly upon excitation, as is expected from the generally accepted theory of PE-formation.[21] The key element of this theory is the so-called line-shape function $g(t)$.[16,21,22] It can

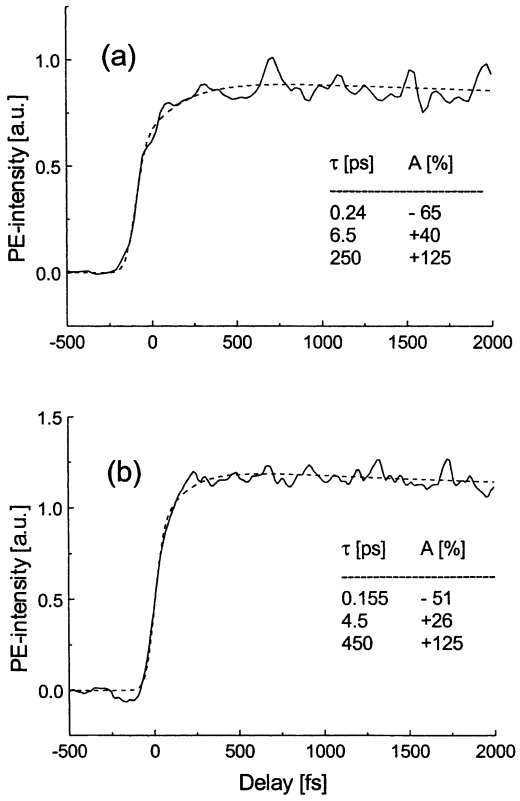

Figure 6. Solid lines: 2PE traces from FMO of *Pr. aestuarii* (a) and *Cl. tepidum* (b) around zero delay, measured at 825 nm. Dashed lines − single trace fit with rise components of 240 fs (a) and 155 fs (b), and slow decay components as indicated. Note that the slow decay times were determined by fitting in a 300 ps delay window.

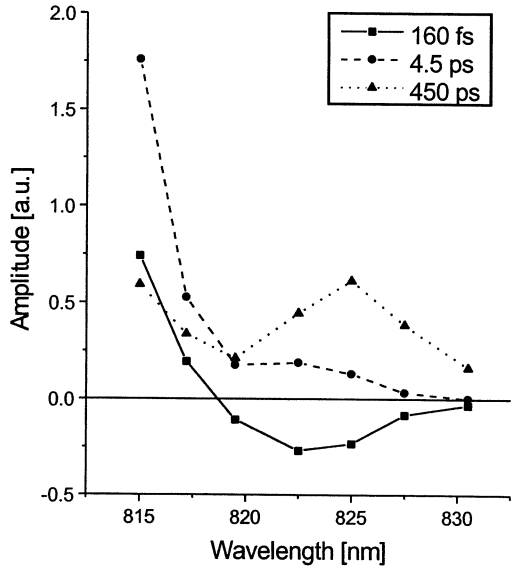

Figure 7. Decay-associated spectra (obtained by global analysis of several decay traces) of 2PE signals from FMO of *Cl. tepidum* in the 815−832 nm wavelength window.

be given over the system-bath correlation function $C(t) = (1/\hbar^2)\langle\hat{U}(t)\hat{U}(0)\rangle$[21,23] which describes the fluctuations of the electronic energy gap

$$g(t) = \int_0^t dt' \int_0^{t'} dt'' C(t'') \tag{4}$$

The 2PE signal depends on the nonlinear induced polarization in the medium[21]

$$S_{PE}(\tau) = \int_{-\infty}^{\infty} |\vec{P}^{(3)}(t,\tau)|^2 \, dt \tag{5}$$

and can be expressed in terms of the third-order molecular response function $R(t_1,t_2,t_3)$ depending only on the line-shape function.[21,24] On the other hand, the absorption spectrum of a single molecule $\alpha(\omega)$, immersed in an environment, can also be completely described in terms of $g(t)$[21]

$$\alpha(\omega) = \frac{1}{2\pi}\int_{-\infty}^{\infty} dt \exp[i(\omega - \omega_{eg})t - g(t)] \tag{6}$$

The line-shape function can be connected[11] to the spectral density of bath states $\rho(\omega) = \tilde{C}(\omega)/\omega^2$ via the Fourier transform of the correlation function $\tilde{C}(\omega) = \int_{-\infty}^{\infty} dt C(t) e^{i\omega t}$

$$g(t) = \tilde{\rho}(0) - \tilde{\rho}(t) - i\Lambda t \tag{7}$$

Here $\tilde{\rho}(t) = 1/2\pi \int_{-\infty}^{\infty} d\omega \rho(\omega) e^{-i\omega t}$ is the Fourier transform of $\rho(\omega)$ in the time domain, $\tilde{\rho}(0)$ characterizes the electron-bath interaction and is simply equal to the Huang−Rhys factor (HRF) S, and $\Lambda = 1/2\pi \int_{-\infty}^{\infty} d\omega \rho(\omega)\omega$ corresponds to the reorganization energy, which represents the spectral shift of the electronic transition between the isolated molecule and that in the environment. Replacing $g(t)$ in eq 6 by eq 7 gives a very familiar form for the absorption profile of an impurity[16]

$$\sigma(\omega) = \frac{1}{2\pi}\int_{-\infty}^{\infty} dt \exp[i(\omega - \omega_{00})t + \tilde{\rho}(t) - \tilde{\rho}(0)] \tag{8}$$

where $\omega_{00} = \omega_{eg} - \Lambda$ denotes the electronic 00-transition. By expanding $\exp[\tilde{\rho}(t)]$ in eq 8 into a Taylor series and inserting the Fourier-images of $[\tilde{\rho}(t)]^n$ (for details see ref [11]), the absorption spectrum can be recast as a sum of the zero-phonon line (ZPL) and the phonon wing (PW).[16] Thus, the bath density of states corresponds exactly to the so-called phonon function: [25] $f(\omega) \equiv \rho(\omega)/2\pi$. It can be easily derived from the measured PW profile using Kukushkin's integral equation,[26] and thus the line-shape function can be constructed. In other words, both absorption spectrum and 2PE-signal (reflecting the time evolution of coherence) originate from the same density of bath states. If the homogeneous absorption spectrum is known, the 2PE signal can be determined, and vice versa. Figure 8 shows $\tilde{\rho}(t)$ and the corresponding $g(t)$, calculated for 1.27 K on the basis of the phonon function derived from the measured PW.[15]

In the impulsive limit (assuming short and well time-separated laser pulses) usually two terms from the third-order molecular correlation function, i.e., R_2 and R_3, are dominating the 2PE-signal. In this limit the PE signal is (see,[21] eq 10.26b)

$$S_{PE}(\tau) = \begin{cases} \{0; (\tau < 0) \\ \exp[-8\mathrm{Re}(g(\tau)) + 2\mathrm{Re}(g(2\tau))] \equiv \\ \qquad \exp[8\mathrm{Re}(\tilde{\rho}(\tau)) - 2\mathrm{Re}(\tilde{\rho}(2\tau)) - 6S]; (\tau \geq 0) \end{cases} \tag{9}$$

This signal, calculated for the FMO complex of *Pr. aestuarii* using $g(t)$ (Figure 8), and S = 0.3,[27] is shown in Figure 9a. As can be seen, at initial delay the 2PE is maximal and relaxes promptly with a characteristic time constant of ∼250 fs corresponding to the relaxation of the line-shape function, reaching a stable level with magnitude of $S_{PE}(\infty) \rightarrow \exp(-6S)$. For an exact calculation of the 2PE signal around zero delay time, where the pulse envelopes are overlapping and cannot be time ordered properly, the sum of all 16 Feynman diagram pathways in the Liouville space should be taking into account.[21]

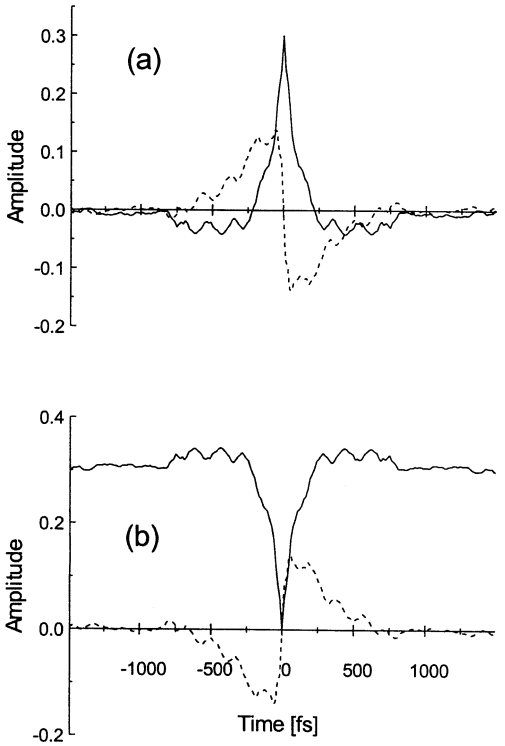

Figure 8. (a) Fourier-image of bath density of states $\tilde{\rho}(t)$, as calculated on the basis of the phonon function derived from the measured PW for FMO of *Pr. aestuarii*.[15] (b) Line-shape function. Solid line − real part, dashed − imaginary part (note that the linear contribution $-i\Lambda t$ is removed; see eq 7 in text). Temperature 1.27 K. Amplitudes are dimensionless.

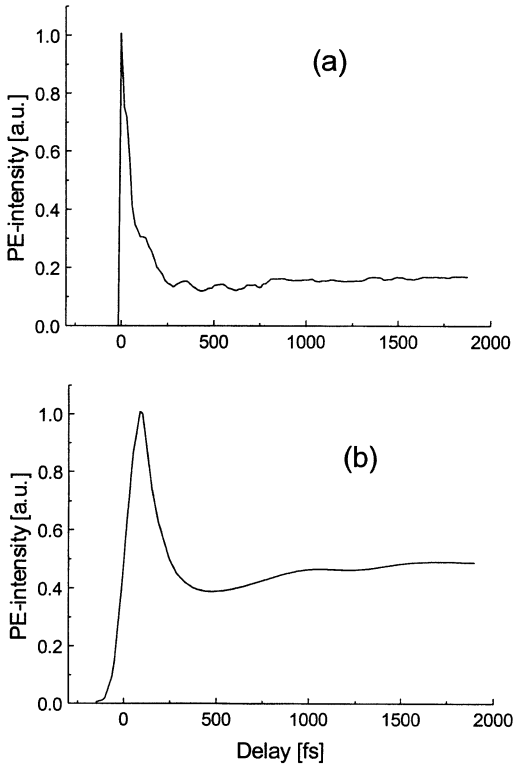

Figure 9. 2PE-signal from FMO of *Pr. aestuarii* around zero delay, calculated within the conventional theory in (a) the impulsive limit, and (b) following excitation with a Gaussian-shaped laser pulse of 80 fs fwhm assuming inhomogeneous broadening of 80 cm^{-1} (for details see text).

The expression for calculating the induced polarization in this case is

$$P^{(3)}(t,\tau) \propto \int_0^\infty dt_3 \int_0^\infty dt_2 \int_0^\infty dt_1 [R_1(t_1,t_2t_3) + R_4(t_1,t_2,t_3)]\chi(t_1 + t_3)E(t - t_3) \times E(t - t_3 - t_2 - t_1)[E^*(t - \tau - t_3 - t_2) + E^*(t + \tau - t_3 - t_2)]\exp[i\omega_L(t_1 + t_3)] + 2\int_0^\infty dt_3 \int_0^\infty dt_2 \int_0^\infty dt_1 [R_2(t_1,t_2,t_3) + R_3(t_1,t_2,t_3)]\chi(t_3 - t_1)E(t - t_3)E(t - t_3 - t_2) \times E^*(t - \tau - t_3 - t_2 - t_1)\exp[i\omega_L(t_3 - t_1)] \quad (10)$$

where $\chi(t)$ is the Fourier-image of the inhomogeneous-broadening function, $E(t)$ is the electrical field pulse envelope, and ω_L is the mean frequency of the laser light. This expression corresponds to eq 11.3 in,[21] adapted to the one-color 2PE irradiated in the $2k_1$-k_2 direction. Figure 9b displays the 2PE signal, calculated beyond the impulsive limit. Here Gaussian-shaped laser pulses with fwhm of 80 fs were used, and inhomogeneous broadening was assumed to be 80 cm^{-1}.[3,15,28] We see that the time evolution of the 2PE is still the same as in the impulsive limit, however the initial peak is smoothed and its amplitude is reduced due to convolution with the finite laser pulse width and finite inhomogeneous broadening. We see that in the framework of the generally accepted theory the photon echo signal *must* display around zero delay an intense peak whose rapid decay corresponds to fast dephasing of the induced polarization due to interaction with the bath. The rather slow small increase of the 2PE-signal after the early decay in this limit reflects a recovery of $\tilde{\rho}(t)$, which follows from Figure 8. Only if we turn off the system−bath interaction by keeping $S = 0$, the photon echo signal will be not accompanied by the intense decaying peak at initial delay. This characteristic behavior of the photon echo signal (particularly APE) was e.g. observed in iron-free myoglobin at 10 K, for which the HRF is very small.[29] Note that in APE-measurements some long-lived "bottleneck" state is involved, which usually is the triplet state of the investigated molecule, and comparison with 2PE-measurements is not straightforward.

In contrast to this theoretically predicted (using presently accepted theory) time evolution of coherence (Figure 9), we do not observe any intense peak with a fast decay in the 2PE kinetics at initial delay. Moreover, the measured signal displays clearly the rapid rise of coherence after impulsive excitation with a characteristic time of 150−250 fs. We conclude that the existing conventional theory of photon echo formation cannot properly describe the observed behavior of the 2PE-signals for FMO, and thus needs to be revised. For that we will use the density matrix formalism in its generalized form, taking into account the non-Markov behavior of the system-bath interaction. The corresponding equations of motion for the reduced density matrix are derived in Appendix A.

IV. Optical Coherence beyond the Markov Limit.

The equation of motion for the reduced density matrix (Appendix A) of the system, interacting with an electrical field $\vec{E}(t)$, can be obtained in the dipole approximation by adding to the Hamiltonian (eq A9) an operator $-\hat{\vec{\mu}}\vec{E}(t)$. In the Condon approximation, the system dipole operator is $\hat{\vec{\mu}} = \vec{\mu}(|1\rangle\langle 0| + |0\rangle\langle 1|)$ (assuming that the molecular dipole moments $\vec{\mu}$ for the

$S_0 \rightarrow S_1$ and $S_1 \rightarrow S_0$ transitions are equal),[30] and we have from eq A17

$$\dot{\rho}_{nm} = -i\omega_{nm}\rho_{nm} - \int_0^t A_{nm}(\tau)e^{-i\omega_{nm}\tau}\,\rho_{nm}(t-\tau)d\tau + \frac{i}{\hbar}\vec{\mu}\vec{E}[\delta_{n,0}\rho_{1m} + \delta_{n,1}\rho_{0m} - \delta_{m,1}\rho_{n0} - \delta_{m,0}\rho_{n1}] \quad (11)$$

where δ is the Kronecker delta. In the Markov limit the second term on the right-hand side of eq 11 should be replaced by $\rho_{nm}\int_0^t A_{nm}(\tau)d\tau$, as shown in Appendix A. The induced polarization is the expectation value of the transition dipole operator

$$\vec{P}(t) = \langle\hat{\vec{\mu}}\rangle = \vec{\mu}(\rho_{01}(t) + \rho_{10}(t)) \quad (12)$$

The applied electrical field can be given generally as

$$\vec{E}(t) = \frac{1}{2}[\vec{\epsilon}(t,\omega,\vec{k},\vec{r})e^{i\omega_{10}t} + \vec{\epsilon}^*(t\omega,\vec{k},\vec{r})e^{-i\omega_{10}t}] \quad (13)$$

where

$$\vec{\epsilon}(t,\omega,\vec{k},\vec{r}) = e^{-i\omega_{10}t}\sum_{i=1}^{N_{\text{puls}}}\vec{A}_i(t)e^{i\omega_i t - i\vec{k}_i\vec{r}} \quad (14)$$

and $\vec{A}_i(t)$ corresponds to the time envelope (a real function) of the i$^{\text{th}}$ laser pulse with frequency ω_i and wave-vector $\vec{k}_i$, and N_{pulse} is the number of applied laser pulses (for the 2PE-case $N_{\text{pulse}} = 2$). For the rotating-wave approximation (RWA) we can write

$$\rho_{01}(t) = \sigma_{01}(t)e^{i\omega_{10}t},\ \rho_{10}(t) = \sigma_{10}(t)e^{-i\omega_{10}t} \quad (15)$$

and for density matrix we obtain the following set of equations

$$\dot{\sigma}_{10} = -\int_0^t A_{10}(\tau)\sigma_{10}(t-\tau)d\tau + \frac{i}{2\hbar}\vec{\mu}\vec{\epsilon}^*(\rho_{00} - \rho_{11}) \quad (\textit{non-Markov limit}) \quad (16a)$$

$$\dot{\sigma}_{10} = -\sigma_{10}\int_0^t A_{10}(\tau)d\tau + \frac{i}{2\hbar}\vec{\mu}\vec{\epsilon}^*(\rho_{00} - \rho_{11}) \quad (\textit{Markov limit}) \quad (16b)$$

$$\sigma_{01} = \sigma_{10}^* \quad (16c)$$

$$\dot{\rho}_{11} = \frac{i}{2\hbar}\vec{\mu}(\sigma_{01}\vec{\epsilon}^* - \sigma_{10}\vec{\epsilon}) \quad (16d)$$

$$\rho_{00} = 1 - \rho_{11} \quad (16e)$$

Note that now the detuning of the electrical field frequency from the electronic $S_0 \rightarrow S_1$ transition $\omega_{10} - \omega_i$ contains the $\vec{\epsilon}(t,\omega,\vec{k},\vec{r})$-factors.

Induced Polarization. Photon echo spectroscopy is a method for monitoring the induced polarization in a medium, whereas removing the effect of free induction decay associated with inhomogeneous broadening of the excited ensemble. Therefore at first we shall consider the time evolution of the polarization created by applying a single laser pulse in both the Markov and non-Markov approximations. For that we need to solve eqs 16a,b assuming very weak excitation ($\rho_{11} = 0$). The applied laser field (eq 14) in this case simplifies to $\vec{\epsilon}(t,\omega,\vec{k},\vec{r}) = \vec{A}(t)e^{i(\omega_L-\omega_{10})t - i\vec{k}\vec{r}}$. At initial conditions we have $\sigma = 0$, $\rho_{00} = 1$, and eq 16b (Markov limit) can be solved immediately[32]

$$\sigma_{10}(t) = \frac{i}{2\hbar}\mu\Theta\int_0^\infty A(t-\tau)\exp[i\Omega(t-\tau) + g(t-\tau) - g(t)]d\tau \quad (17)$$

where $\Omega = \omega_{10} - \omega_L$ is the detuning of the laser field from the electronic transition, $\Theta = \cos(\vec{\mu},\vec{A})$, and $g(t) = \int_0^t dt'\int_0^{t'} dt''A_{10}(t'')$ is the line-shape function. For solving eq 16a (non-Markov limit), we can rewrite it equivalently in the form of a convolution integral

$$\hat{a}\otimes\sigma_{10} = \frac{i}{2\hbar}\mu\Theta\epsilon^* \quad (18)$$

where the operator $\hat{a}(t)$ is given by

$$\hat{a}(t) = \frac{d}{dt}\delta(t) + \theta(t)A_{10}(t) \quad (19)$$

Here, $\delta(t)$ is the Dirac δ-function, and $\theta(t)$ is the Heavyside step function. Thus the solution of eq 18 for the same initial conditions is simply a convolution of the excitation field with the reciprocal operator $\hat{a}^{-1}(t)$

$$\sigma_{10} = \frac{i}{2\hbar}\mu\Theta(\hat{a}^{-1}\otimes\epsilon^*) \quad (20)$$

This operator can be found using the Laplace transform technique which results in

$$\hat{a}^{-1}(t) = \frac{1}{2\pi}\theta(t)\int_{-\infty}^{\infty} d\omega e^{i\omega t}\frac{1}{i\omega + \tilde{\tilde{A}}_{10}(\omega)} \quad (21)$$

where

$$\tilde{\tilde{A}}_{10}(\omega) = \int_0^\infty A_{10}(t)e^{-i\omega t}dt \quad (22)$$

is the Fourier−Laplace transform of the system-bath correlation function. Beyond the Markov limit we finally get

$$\sigma_{10}(t) = \frac{i}{4\pi\hbar}\mu\Theta\int_0^\infty d\tau A(t-\tau)\exp[i\Omega(t-\tau)]\int_{-\infty}^{\infty} d\omega\, e^{i\omega\tau}/[i\omega + \tilde{\tilde{A}}_{10}(\omega)] \quad (23)$$

Both expressions, eqs 17 and 23, give the same result in the limiting case $S \rightarrow 0$, i.e., in the absence of system-bath interactions

$$\sigma_{10}(t)|_{S\rightarrow 0} = \frac{i}{2\hbar}\mu\Theta\int_0^\infty d\tau A(t-\tau)e^{i\Omega(t-\tau)} \quad (24)$$

Equations 17, 23, and 15, allow to calculate the induced polarization (eq 12). For going beyond the Markov limit we need to calculate $\tilde{\tilde{A}}_{10}(\omega)$. This can be done directly using the Fourier image of the bath density of states $\tilde{A}_{10}(\omega) = \omega^2\rho(\omega)$ (see previous section). However, from the symmetrical properties of the real and imaginary parts of $A_{10}(t)$ (Appendix A) it follows that

$$\text{Re}(\tilde{\tilde{A}}_{10}(\omega)) = \frac{1}{2}\tilde{A}_{10}(\omega) \quad (25)$$

and the imaginary part can be obtained from its real part using the Kramers−Kronig relationship[11,32]

$$\text{Im}(\tilde{\tilde{A}}_{10}(\omega)) = \frac{1}{\pi}PP\int_{-\infty}^{\infty}\frac{\tilde{A}_{10}(\Omega)}{\Omega - \omega}d\Omega \quad (26)$$

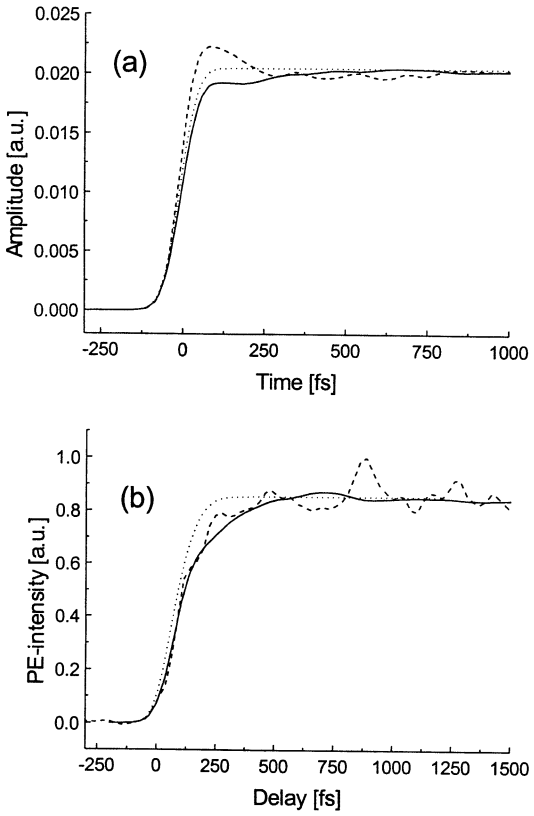

Figure 10. (a) Time evolution of the induced polarization calculated within the Markov limit (dashed), beyond the Markov limit (solid), and in the absence of system-bath interaction (dots). Excitation: Gaussian-shaped pulse (centered at $t = 0$) with duration of 80 fs fwhm (laser frequency in exact resonance with electronic $S_0 \rightarrow S_1$ transition). (b) 2PE-signal (solid), calculated beyond the Markov limit (following eq 30) for FMO of *Pr. aestuarii*. For better comparison, the experimentally measured signal is also shown (dashed). The dotted line corresponds to the 2PE-signal in the absence of system-bath interaction (zero Huang−Rhys factor). The excitation conditions the same as for Figure 9.

Figure 10a shows the calculated time evolution of the induced polarization (envelope) in both the Markov and non-Markov limits, taken at resonance $\Omega = 0$ and for our experimental conditions. As can be seen, by taking into account the finite time of the system-bath interaction, already in the first order of the applied electrical field the induced polarization exhibits *a delayed growing-in* that appears in the PE-signal as a rise component. The induced polarization reaches its stationary value after 400−600 fs. This behavior differs principally from the Markov limit, where the induced polarization around zero delay already reaches its maximum (cf., Figure 9b, calculated 2PE). The growth of coherence should be even more pronounced in the 2PE-signal, which corresponds to polarization in the third order of the applied field.

Photon Echo. Deriving the general equation for the third-order induced polarization beyond the Markov limit suitable for describing nonlinear time-resolved experiments of different kinds, is carried out in Appendix B. Here, we apply this expression for conventional one-color 2PE corresponding to our experimental conditions. For that we specify the applied fields choosing $N_{\text{pulse}} = 2$ (eq 14), assuming that the second laser pulse is delayed by a time delay τ, and for both pulses we assume equal time envelopes $A(t)$ and the same polarization ($\Theta_1 = \Theta_2 \equiv \Theta$)

$$\epsilon_\mu(t,\Omega,\vec{k},\vec{r}) = \Theta[A(t)e^{-i\Omega t - i\vec{k}_1\vec{r}} + A(t-\tau)e^{-i\Omega t - i\omega_L\tau - i\vec{k}_2\vec{r}}] \quad (27)$$

In eq B9 the off-diagonal elements of the density matrix depend on the laser field products $\epsilon\epsilon\epsilon^*$, $\epsilon\epsilon^*\epsilon$, $\epsilon^*\epsilon^*\epsilon$, and $\epsilon^*\epsilon\epsilon^*$ which corresponds to 4 directions in k-space; we will collect the corresponding terms only for the $2\vec{k}_1 - \vec{k}_2$ direction in which the 2PE signals were measured

$$\vec{P}^{(3)}(t) = \vec{\mu}(\rho_{01}(t)e^{-i(2\vec{k}_1-\vec{k}_2)\vec{r}} + \rho_{10}(t)e^{i(2\vec{k}_1-\vec{k}_2)\vec{r}}) \quad (28)$$

In the next step, we perform an integration over an inhomogeneously broadened ensemble of molecules, assuming a Gaussian distribution of electronic transitions

$$G(\omega_{10}) = \sqrt{\frac{\alpha}{\pi}}\frac{1}{\Delta\omega_{00}}\exp\left[-\frac{\alpha}{2}\left(\frac{\omega_{00}-\omega_{10}}{\Delta\omega_{00}}\right)^2\right] \quad (29)$$

where ω_{00} is the mean transition frequency, $\alpha = 4ln(2)$, $\Delta\omega_{00}$ is the fwhm of the distribution with area normalized to 1. Finally, for the third-order induced polarization irradiated in the $2\vec{k}_1 - \vec{k}_2$ direction (*photon echo pulse*), from eq B9 we have

$$\begin{aligned}\vec{P}^{(3)}(t) = -\frac{1}{2\hbar^3}\vec{\mu}\mu^3\Theta^3\{&\int_0^\infty dt'\int_0^\infty dt''\int_0^\infty dt'''A(t-t')\times \\ &A(t-t'-t'')A(t-\tau-t'-t''-t''')\chi(t'''-t') \\ &\times \mathrm{Im}\{b^*(t')b(t''')\exp[i\omega_L(t+\tau)+i\Omega(t'-t''')- \\ &i(2\vec{k}_1-\vec{k}_2)\vec{r}]\}\} \\ +&\int_0^\infty dt'\int_0^\infty dt''\int_0^\infty dt'''A(t-t')A(t-\tau-t'-t'')\times \\ &A(t-t'-t''-t''')\chi(t'''+t') \\ &\times \mathrm{Im}\{b^*(t')b^*(t''')\exp[i\omega_L(t+\tau)+i\Omega(t'+t''')- \\ &i(2\vec{k}_1-\vec{k}_2)\vec{r}]\}\} \quad (30)\end{aligned}$$

where $\Omega = \omega_{00} - \omega_L$ is now the detuning of the laser frequency from the mean transition frequency of the inhomogeneously broadened ensemble, and $\chi(t) = \exp[-(\Delta\omega_{00}/2)^2t^2/\alpha]$ is the Fourier-image of the distribution function in the time domain. From this expression it follows that the induced polarization is a real function.

Calculation of 2PE-Signal for FMO. We now go on to calculate the 2PE-signal using the same parameters as before for the Markov limit (see section III, and Figure Caption 9). The calculated 2PE-signal at 825 nm (center of red peak in absorption spectrum) is shown in Figure 10b; for a better comparison the measured signal is also shown. We see that the 2PE-signal, calculated beyond the Markov limit, corresponds perfectly to the experimentally measured trace,[33] and displays a *rise component* with a characteristic time constant of ~250 fs. Comparison with the 2PE-trace, calculated in the absence of system-bath interaction ($S = 0$, which results in $b(t) = 1$; see Appendix B) indicates clearly a growing-in of coherence in the real system. The important point here is that the time delay in the development of coherence is caused by a finite system-bath interaction time—i.e., the behavior of the system depends on its past history, and coherence does not appear immediately after excitation.

V. Conclusions

In this experimental and theoretical work, we demonstrated that for a detailed understanding of the interaction of molecules

with an environment it is principally necessary to take into account their finite interaction time. We show here that beyond the Markov limit this interaction leads to a system-bath memory effect, which appears particularly in the photon echo signal as a delayed growing-in of coherence. In other words, the system is damped due to coupling with the bath, and cannot follow the excitation promptly—thus, the appearance of induced polarization will be delayed. As demonstrated, the conventional theory of photon echo formation fails in describing the development of the induced polarization in the time domain comparable to the system-bath interaction time, and predicts an erroneous result in this case. In contrast to that, taking the system-bath memory effect into consideration leads to a correct description of the experimental observations.

We report here on the experimental discovery of the growing-in of coherence in a particular system, the so-called FMO antenna complex. However, from the theory developed here, it follows that this effect should be quite general. Its clear manifestation in experimental observations will be dependent on many parameters however (temperature, HRF, structure of the environment etc.), that determine the time range of the system-bath interaction and the correlation function itself. In Appendix A it is pointed out that the correlation between ground and excited states enters only into the real part, whereas its imaginary part depends on the correlations of bath variables only in their respective electronic states. The presence of correlation between electronic states (or their absence) can influence significantly the dynamics of the system-bath interaction. Thus, it will be important to perform further detailed experimental investigations in other systems to better understand under which conditions this effect is significant for describing the dynamics of a system. In conclusion, we also note that at this stage it is not clear if and how this phenomenon may affect the light-harvesting function of natural photosynthetic antennae, especially at room temperature.

Acknowledgment. This work was supported by Deutsche Forschungsgemeinschaft (Sonderforschungsbereich 189) and partly by the European Community TMR network on green bacterial photosynthesis Grant No. FM-RX-CT960081.

Appendix A.

Evaluation of the Equation for the Reduced Density Matrix beyond the Markov Limit. We will start from the Liouville equation for the density operator in the Schrödinger picture

$$i\hbar\frac{\partial\hat{\rho}}{\partial t} = [\hat{H},\hat{\rho}] \tag{A1}$$

where the time-dependent Hamiltonian is the sum of the system and bath Hamiltonians (which are independent of time) $\hat{H}_0 = \hat{H}_S + \hat{H}_B$, and the term $\hat{V}(t) \equiv \hat{H}_{S-B}(t)$ that describes a time-dependent perturbation due to their interaction

$$\hat{\mathrm{H}}(t) = \hat{\mathrm{H}}_0 + \hat{\mathrm{V}}(t) \tag{A2}$$

Using the unitary transform

$$\hat{\rho}_{\mathrm{int}}(t) = e^{i/\hbar\hat{\mathrm{H}}_0 t}\hat{\rho}(t)e^{-i/\hbar\hat{\mathrm{H}}_0 t} \tag{A3}$$

we can switch eq A1 to the interaction picture

$$i\hbar\frac{\partial\hat{\rho}_{\mathrm{int}}}{\partial t} = [\hat{V}_{\mathrm{int}},\hat{\rho}_{\mathrm{int}}] \tag{A4}$$

and by formal integration we get

$$\hat{\rho}_{\mathrm{int}}(t) = \hat{\rho}_{\mathrm{int}}(0) - \frac{i}{\hbar}\int_0^t[\hat{\mathrm{V}}_{\mathrm{int}}(x),\hat{\rho}_{\mathrm{int}}(x)]dx \tag{A5}$$

Plugging eq A5 into eq A4 we get

$$\frac{\partial\hat{\rho}_{\mathrm{int}}}{\partial t} = -\frac{i}{\hbar}[\hat{\mathrm{V}}_{\mathrm{int}}(t),\hat{\rho}(0)] - \frac{1}{\hbar^2}\int_0^t[\hat{\mathrm{V}}_{\mathrm{int}}(t),[\hat{\mathrm{V}}_{\mathrm{int}}(x),\hat{\rho}_{\mathrm{int}}(x)]]dx \tag{A6}$$

where $\hat{\rho}_{\mathrm{int}}(0) \equiv \hat{\rho}(0)$. A reduced density operator $\hat{\rho}^S_{\mathrm{int}}$ corresponding to the observable system can be obtained from $\hat{\rho}_{\mathrm{int}}$ by taking the trace over the bath variables $\hat{\rho}^S_{\mathrm{int}}(t) = Tr_B(\hat{\rho}_{\mathrm{int}}(t))$, and thus, the equation for the reduced density matrix is

$$\frac{\partial\hat{\rho}^S_{\mathrm{int}}}{\partial t} = -\frac{i}{\hbar}Tr_B([\hat{\mathrm{V}}_{\mathrm{int}}(t),\hat{\rho}(0)]) - \frac{1}{\hbar^2}\int_0^t Tr_B([\hat{\mathrm{V}}_{\mathrm{int}}(t),[\hat{\mathrm{V}}_{\mathrm{int}}(x),\hat{\rho}_{\mathrm{int}}(x)]])dx \tag{A7}$$

Note that by performing the integration we assumed that up to time point $t = 0$ the system and bath are not-interacting, and thus they are not correlated. In that case the total density operator is a product of the system density operator and the bath density operator $\hat{\rho}(0) = \hat{\rho}^S(0)\cdot\hat{\rho}^B(0)$. Supposing that the bath has an infinitely large number of degrees of freedom as compared to the system, we can assume that for $t > 0$ $\hat{\rho}_{\mathrm{int}}(x) = \hat{\rho}^S_{\mathrm{int}}(x)\cdot\hat{\rho}^B(0)$

$$\frac{\partial\hat{\rho}^S_{\mathrm{int}}}{\partial t} = -\frac{i}{\hbar}Tr_B([\hat{\mathrm{V}}_{\mathrm{int}}(t),\hat{\rho}^S(0)\cdot\hat{\rho}^B(0)]) - \frac{1}{\hbar^2}\int_0^t Tr_B([\hat{\mathrm{V}}_{\mathrm{int}}(t),[\hat{\mathrm{V}}_{\mathrm{int}}(x),\hat{\rho}^S_{\mathrm{int}}(x)\cdot\hat{\rho}^B(0)]])dx \tag{A8}$$

We now go on to evaluate the equation of motion for the density matrix describing a single molecule immersed into an environment. However, this consideration can be straightforwardly extended to any ensemble of coupled molecules whose density operator can be separated into the system and the bath operators. For linear electron-bath coupling the corresponding Hamiltonian (we consider the molecules within the two-level electronic approximation) can be given in general form as

$$\hat{H} = \hat{H}_e + \hat{H}_g + \hat{H}_B \equiv |1\rangle\hbar\omega_e\langle 1| + |0\rangle\hbar\omega_g\langle 0| + |1\rangle\langle 1|\hat{F}_1 + |0\rangle\langle 0|\hat{F}_0 + \hat{H}_B \tag{A9}$$

where we have neglected the off-diagonal system-bath interaction that causes an attenuation of excitation due to the T_1-process. The bath operators $\hat{F}_1$, $\hat{F}_0$ correspond to the S_1 and S_0 states (we assume that they are Hermitian) and act only on the bath variables, and ω_e, ω_g are the electronic energies in the excited S_1 and ground S_0 states, described by stationary wave functions $|1\rangle$ and $|0\rangle$, respectively. Further, we assume that the average expectation value of the bath operators is zero. In this case the system-bath interaction can be written as

$$\hat{V} = \sum_i \hat{Q}_i\hat{F}_i, \tag{A10}$$

where index $i \in [0,1]$, and system operators are $\hat{Q}_i = |i\rangle\langle i|$. Because the bath and system operators act on independent variables, in the interaction picture the operator $\hat{V}_{\mathrm{int}}(t)$ has the same structure: $\hat{V}_{\mathrm{int}}(t) = \sum_i\hat{Q}_i(t)\hat{F}_i(t)$, where

$$\hat{Q}_i(t) = e^{i/\hbar\hat{H}_S t}\hat{Q}_i e^{-i/\hbar\hat{H}_S t},\ \hat{F}_i(t) = e^{i/\hbar\hat{H}_B t}\hat{F}_i e^{-i/\hbar\hat{H}_B t}$$

are corresponding Heisenberg operators of $\hat{Q}_i$ and $\hat{F}_i$, respectively. Using commutability of the system and bath operators, for the trace under integral in eq A8, we get

$$Tr_B([\hat{V}_{\text{int}}(t),[\hat{V}_{\text{int}}(x),\ \hat{\rho}^S_{\text{int}}(x)\cdot\hat{\rho}^B(0)]]) = \sum_{i,j=0}^{1}\{(\hat{Q}_i(t)\hat{Q}_j(x)\hat{\rho}^S_{\text{int}}(x) - \hat{Q}_i(t)\hat{\rho}^S_{\text{int}}(x)\hat{Q}_j(x)) \quad \text{(A11)}$$

$$\cdot\langle\hat{F}_i(t)\hat{F}_j(x)\rangle - (\hat{Q}_i(x)\hat{\rho}^S_{\text{int}}(x)\hat{Q}_i(t) - \hat{\rho}^S_{\text{int}}(x)\hat{Q}_j(x)\hat{Q}_i(t))\langle\hat{F}_j(x)\hat{F}_i(t)\rangle\}$$

The first term in eq A8 vanishes identically because the average values of the bath operators are zero. The equation for the density matrix can be obtained from eq A8 by taking the matrix elements between eigenstates of the system $(\hat{\rho}^S_{\text{int}})_{nm} = \langle n|\hat{\rho}^S_{\text{int}}|m\rangle$. Taking into account that the matrix element of the system operators in our case are $\langle n|\hat{Q}_i(t)|m\rangle = e^{i(\omega_n-\omega_m)t}\delta_{n,i,m}$ (where δ is the Kronecker delta, and $n,m \in [0,1]$), and using eq A11, in the interaction picture we obtain for the density matrix

$$\left(\frac{\partial\hat{\rho}^S_{\text{int}}}{\partial t}\right)_{nm} = -\frac{1}{\hbar^2}\int_0^t (\langle\hat{F}_n(t)\hat{F}_n(x)\rangle - \langle\hat{F}_n(t)\hat{F}_m(x)\rangle - \langle\hat{F}_n(x)\hat{F}_m(t)\rangle + \langle\hat{F}_m(x)\hat{F}_m(t)\rangle)(\rho^S_{\text{int}}(x))_{nm}dx \quad \text{(A12)}$$

Because the correlation functions are stationary[34] (i.e., $\langle\hat{F}(t)\hat{F}(x)\rangle = \langle\hat{F}(t-x)\hat{F}(0)\rangle$), by changing of variables to $\tau = t - x$, eq A12 can be rewritten in the form

$$\left(\frac{\partial\hat{\rho}^S_{\text{int}}}{\partial t}\right)_{nm} = -\int_0^t A_{nm}(\tau)(\hat{\rho}^S_{\text{int}}(t-\tau))_{nm}d\tau \quad \text{(A13)}$$

where $A(\tau)$ denotes a total correlation function that includes the sum of the correlation functions for bath operators in the ground state, the excited state, and the correlations between ground and excited states

$$A_{nm}(\tau) = \frac{1}{\hbar^2}(\langle\hat{F}_n(\tau)\hat{F}_n(0)\rangle - \langle\hat{F}_n(\tau)\hat{F}_m(0)\rangle - \langle\hat{F}_n(0)\hat{F}_m(\tau)\rangle + \langle\hat{F}_m(0)\hat{F}_m(\tau)\rangle) \quad \text{(A14)}$$

After simple transformations the correlation function $A_{nm}(\tau)$ can be written in the form

$$A_{nm}(\tau) = \frac{1}{\hbar^2}\{\langle\hat{F}_n(\tau)\hat{F}_n(0)\rangle + \langle\hat{F}_m(\tau)\hat{F}_m(0)\rangle^* - 2\text{Re}\langle\hat{F}_n(\tau)\hat{F}_m(0)\rangle\} \quad \text{(A15)}$$

and we see that $A_{00}(\tau) = A_{11}(\tau) \equiv 0$, $A_{nm}(\tau) = A_{nm}(-\tau)^*$, and $A_{01}(\tau) = A_{10}(\tau)^*$. The correlation function can be separated into its real and imaginary parts: $A_{10}(\tau) = A'_{10}(\tau) + iA''_{10}(\tau)$. The real part is an even function $A'_{10}(\tau) = A'_{10}(-\tau)$, whereas $A''_{10}(\tau) = -A''_{10}(-\tau)$ is an odd function (the same is valid also for $A_{01}(\tau)$). From eq A15, it follows that both the correlations of bath variables within a single electronic state, and also between different states (the last term in eq A15) contribute to the real part of the overall correlation function $A(\tau)$, whereas the imaginary part depends only on the correlation of bath variables in each of their respective electronic states alone.

In standard quantum theory of relaxation,[34] developed in the Markov limit, the system density matrix depends only on its present value $\hat{\rho}^S(t-\tau) \approx \hat{\rho}^S(t)$ which allows to separate it from the integral in eq A13 in the following manner

$$\left(\frac{\partial\hat{\rho}^S_{\text{int}}}{\partial t}\right)_{nm} \cong -(\hat{\rho}^S_{\text{int}})_{nm}\int_0^t A_{nm}(\tau)d\tau \quad \text{(A16)}$$

Moreover, the correlation function is assumed to be decaying very fast, and the upper integration limit is actually extended to infinity which corresponds to the Bloch limit. In other words, the behavior of the system is described as a "coarse-grained" average, where the time intervals between observations are assumed to be much larger as compared to the characteristic intrinsic bath memory time. If integration is performed to a finite time point t only, then we can describe the system behavior taking into account also some features of the finiteness of the system-bath interaction (still staying in the Markov limit however), and the time evolution of the system can be traced in more detail. As can be seen, the equation of motion for the reduced density matrix in the Markov limit (eq A16) follows simply from the general expression of motion for the density matrix, eq A13, by expanding the density operator into a Taylor series around time point t and keeping the first term only: $\hat{\rho}^S_{\text{int}}(t-\tau) = \hat{\rho}^S_{\text{int}}(t) - 1/1!\ \hat{\rho}^S_{\text{intm}}(t)\cdot\tau + \cdots$. Thus we see, that eq A16 is only a *zero-order approximation* of eq A13.

Switching back to the Schrödinger picture using the unitary transform eq A3, we obtain an equation of motion for the reduced density matrix beyond the Markov limit

$$\frac{\partial\rho^S_{nm}}{\partial t} = -i\omega_{nm}\rho^S_{nm} - \int_0^t A_{nm}(\tau)e^{-i\omega_{nm}\tau}\rho^S_{nm}(t-\tau)d\tau \quad \text{(A17)}$$

($\omega_{nm} = \omega_n - \omega_m$), whereas in the Markov limit we have from eq A16

$$\frac{\partial\rho^S_{nm}}{\partial t} = -i\omega_{nm}\rho^S_{nm} - \rho^S_{nm}\int_0^t A_{nm}(\tau)d\tau \quad \text{(A18)}$$

Note that similar equations of motion were obtained earlier in ref 35 using the cumulant expansion technique.[36] In that work, the two different forms of the equations of motion were derived using different time ordering prescriptions − the chronological ordering prescription that leads to eq A17, and the partial ordering prescription results in eq A18. Moreover, it was pointed out that both time ordering prescriptions are equal in principle (but only if the corresponding operators are evaluated to infinite order). However, following truncation in the second order, as is usually done in the literature, they lead to a different behavior of the system-bath interaction. From our analysis it follows that the direct evaluation of the equation of motion using the density matrix formalism is free from this inequality since we get an exact solution, and gives a clear physical meaning for both expressions. The first takes into account the finite system-bath correlation time and the past history, and is thus truly non-Markovian (eq A13). The second one (eq A 16) fulfills the Bloch limit but does not account for the system-bath correlation and ignores the past event. It thus essentially follows a Markovian limit.

Appendix B.

Third-Order Induced Polarization. The induced polarization $\vec{P}(t,E)$ can be evaluated from system eqs 16a, 16c−e up to any order in the applied field E using perturbation theory. In first order, assuming weak excitation ($\rho_{00} \approx 1$, $\rho_{11} \approx 0$), the solution is given by eq 23 which we shall rewrite as

$$\sigma^{(1)}_{10}(t) = \frac{i}{2\hbar}\mu\int_0^\infty \epsilon^*_\mu(t-t')b(t')dt', \quad \text{(B1)}$$

where $\epsilon_\mu(t,\omega,\vec{k},\vec{r}) \equiv \sum_i^{N_{puls}} \cos(\vec{\mu},\vec{A}_i)A_i(t)e^{i(\omega_i-\omega_{10})t-i\vec{k}_i\vec{r}}$ is the projection of the laser field on the transition dipole moment vector, and $b(t) = \int_{-\infty}^{\infty} d\omega e^{i\omega t}/[i\omega + \tilde{\tilde{A}}_{10}(\omega)]$ (see eq 21). In the second-order, we have for the diagonal element

$$\dot{\rho}_{11}^{(2)}(t) = \frac{\mu^2}{4\hbar^2}[\epsilon_\mu^*(t)\int_0^\infty \epsilon_\mu(t-t')b^*(t')dt' + c.c.] \quad \text{(B2)}$$

whose solution at initial conditions $\rho_{11}^{(2)} = 0$ is

$$\rho_{11}^{(2)}(t) = \frac{\mu^2}{4\hbar^2} \times [\int_0^\infty dt' \int_0^\infty dt'' \epsilon_\mu^*(t-t')\epsilon_\mu(t-t'-t'')b^*(t'') + c.c] \quad \text{(B3)}$$

Plugging this into eq 16a allows us to calculate the off-diagonal elements of the density matrix in third order

$$\dot{\sigma}_{10}^{(3)}(t) = -\int_0^t A_{10}(\tau)\sigma_{10}^{(3)}(t-\tau)d\tau + \frac{i}{2\hbar}\mu\epsilon_\mu^*(t)[1-2\rho_{11}^{(2)}(t)] \quad \text{(B4)}$$

We see that

$$\sigma_{10}^{(3)}(t) = \sigma_{10}^{L}(t) + \sigma_{10}^{NL}(t) \quad \text{(B5)}$$

where the index "*L*" denotes a contribution that is linear with the applied field

$$\dot{\sigma}_{10}^{L}(t) = -\int_0^t A_{10}(\tau)\sigma_{10}^{L}(t-\tau)d\tau + \frac{i}{2\hbar}\mu\epsilon_\mu^*(t) \quad \text{(B6)}$$

with a solution which is given by eq B1, and a third-order nonlinear contribution, denoted by index "*NL*"

$$\dot{\sigma}_{10}^{NL}(t) = -\int_0^t A_{10}(\tau)\sigma_{10}^{NL}(t-\tau)d\tau - \frac{i}{\hbar}\mu\epsilon_\mu^*(t)\rho_{11}^{(2)}(t) \quad \text{(B7)}$$

Its solution is

$$\sigma_{10}^{NL}(t) = -\frac{i}{4\hbar^3}\mu^3[\int_0^\infty dt' \int_0^\infty dt'' \int_0^\infty dt''' \epsilon_\mu^*(t-t') \times \epsilon_\mu^*(t-t'-t'')\epsilon_\mu(t-t'-t''-t''')b(t')b^*(t''') + \int_0^\infty dt' \int_0^\infty dt'' \int_0^\infty dt''' \epsilon_\mu^*(t-t')\epsilon_\mu(t-t'-t'') \times \epsilon_\mu^*(t-t'-t''-t''')b(t')b(t''')] \quad \text{(B8)}$$

Both of these contributions correspond to different propagations of the induced polarization (see eq 14), and in mixed directions such as $2\vec{k}_i \pm \vec{k}_j$ the linear part of the polarization will not contribute. Taking into account eqs 12 and 15, we obtain a general expression for the nonlinear induced polarization beyond the Markov limit

$$\vec{P}^{(3)}(t) = \frac{i}{4\hbar^3}\vec{\mu}\mu^3\{e^{i\omega_{10}t}[\int_0^\infty dt' \int_0^\infty dt'' \int_0^\infty dt''' \epsilon_\mu(t-t') \times \epsilon_\mu(t-t'-t'')\epsilon_\mu^*(t-t'-t''-t''')b^*(t')b(t''') + \int_0^\infty dt' \int_0^\infty dt'' \int_0^\infty dt''' \epsilon_\mu(t-t')\epsilon_\mu^*(t-t'-t'') \times \epsilon_\mu(t-t'-t''-t''')b^*(t')b^*(t''')] - e^{-i\omega_{10}t}[\int_0^\infty dt' \int_0^\infty dt'' \int_0^\infty dt''' \epsilon_\mu^*(t-t') \times \epsilon_\mu^*(t-t'-t'')\epsilon(t-t'-t''-t''')b(t')b^*(t''') + \int_0^\infty dt' \int_0^\infty dt'' \int_0^\infty dt''' \epsilon_\mu^*(t-t')\epsilon_\mu(t-t'-t'') \times \epsilon_\mu^*(t-t'-t''-t''')b(t')b(t''')]\} \quad \text{(B9)}$$

This expression gives a basis for the calculation of different kinds of PE-signals (2PE, 3PE, 3PE-peak-shift), transient grating, and pump−probe experiments beyond the Markov limit by the appropriate choice of applied fields and propagation directions.

References and Notes

(1) Fenna, R. E.; Matthews, B. W. *Nature* **1975**, *258*, 573.

(2) Li, Y.-F.; Zhou, W.; Blankenship, R. E.; Allen, J. P. *J. Mol. Biol.* **1997**, *271*, 456.

(3) Louwe, R. J. W.; Vrieze, J.; Hoff, A. J.; Aartsma, T. J. *J. Phys. Chem. B* **1997**, *101*, 11280.

(4) Generally speaking, pigment #3 is not strictly isolated: FMO is a trimer, and so it contains three pigments #3. However, its interaction with other pigments in the FMO subunits is very weak (up to ~7 cm^{-1}) which does not perturb markedly the excitation localization.

(5) Van Amerongen, H.; Struve, W. S. *J. Phys. Chem.* **1991**, *95*, 9020.

(6) Buck, D. R.; Savikhin, S.; Struve, W. S. *Biophys. J.* **1997**, *72*, 24.

(7) Vulto, S. I. E.; Neerken, S.; Louwe, R. J. W.; de Baat, M. A.; Amesz, J.; Aartsma, T. J. *J. Phys. Chem. B* **1998**, *102*, 10 630.

(8) Francke, C.; Amesz, J. *Photosynth. Res.* **1997**, *52*, 137.

(9) Prokhorenko, V. I.; Steensgaard, D. B.; Holzwarth, A. R. *Biophys. J.* **2000**, *79*, 2105.

(10) For a two-level system in the Bloch model, this dephasing constant is related to the dephasing time T_2 as $\tau = T_2/4$.

(11) Prokhorenko, V. I.; Holzwarth, A. R. *J. Phys. Chem. B* **2000**, *104*, 11 563.

(12) Vulto, S. I. E.; Streltsov, A. M.; Aartsma, T. J. *J. Phys. Chem. B* **1997**, *101*, 4845.

(13) Vulto, S. I. E.; de Baat, M. A.; Neerken, S.; Nowak, F. R.; van Amerongen, H.; Amesz, J.; Aartsma, T. J. *J. Phys. Chem. B* **1999**, *103*, 8153.

(14) Savikhin, S.; Buck, D. R.; Struve, W. S. *Chem. Phys.* **1997**, *223*, 303.

(15) Wendling, M.; Pullerits, T.; Przyjalgowski, M. A.; Vulto, S. I. E.; Aartsma, T. J.; van Grondelle, R.; van Amerongen, H. *J. Phys. Chem. B* **2000**, *104*, 5825.

(16) Personov, R. I. In *Spectroscopy and Excitation Dynamics of Condensed Mol. Systems*; Agranovich, V. M., Hochstrasser, R. M., Eds.; Publishing Company: Amsterdam, 1983; p 555.

(17) Saikan, S.; Nakabayashi, T.; Kanematsu, Y.; Imaoka, A. *J. Chem. Phys.* **1988**, *89*, 4609.

(18) Saikan, S. *J. Luminesc.* **1992**, *53*, 147.

(19) Saikan, S.; Imaoka, A.; Kanematsu, Y.; Kishida, T. *Chem. Phys. Lett.* **1989**, *162*, 217.

(20) Aartsma, T. J.; Louwe, R. J. W.; Schellenberg, P. In *Biophysical Techniques in Photosynthesis. Advances in Photosynthesis*, Vol.3; Amesz, J., Hoff, A. J., Eds.; Kluwer Academic Publishers: Dordrecht, 1996; p 109.

(21) Mukamel, S. *Principles of Nonlinear Optical Spectroscopy*; Oxford University Press: New York, 1995.

(22) Maradudin, A. A. In *Solid State Phys. 18*; Seitz, F., Turnbull, D., Eds.; 1966; p 392.

(23) YI, J. Y.; Mukamel, S. *J. Chem. Phys.* **1991**, *94*, 179.

(24) Cho, M.; Yu, J.-Y.; Joo, T.; Nagasawa, Y.; Passino, S. A.; Fleming, G. R. *J. Phys. Chem.* **1996**, *100*, 11 944.

(25) Osad'ko, I. S. *Usp. Fiz. Nauk* **1979**, *128*, 31.

(26) Kukushkin, L. S. *Fiz. Tverd. Tela* **1965**, *7*, 54.

(27) Johnson, S. G.; Small, G. J. *J. Phys. Chem.* **1991**, *95*, 471.

(28) Johnson, S. G.; Small, G. J. *Chem. Phys. Lett.* **1989**, *155*, 371.

(29) Lin, J. W.-I.; Tada, T.; Saikan, S.; Kushida, T.; Tani, T. *Phys. Rev. B* **1991**, *44*, 7356.

(30) Henceforth index "s" for denoting of the system density matrix is omitted.

(31) For clarity of presentation, we omitted the term which describes the propagation direction of the induced polarization.

(32) Renger, T.; May, V. *Phys. Rev. Lett.* **2000**, *84*, 5228.

(33) The calculated signal does not display the characteristic oscillations that are present in the measured traces. For numerical modeling a density of bath states, recovered from the measured site-selective fluorescence spectrum (see section. III) was used. In this spectrum the corresponding contributions of vibrational states of BChl *a* molecule that appear in 2PE signal as oscillations, are not resolved. Note that the same is valid for the results of calculations displayed in Figure 8, 9.

(34) Blum, K. *Density Matrix Theory and Applications*; Plenum Press: New York, 1981.

(35) Mukamel, S. *Chem. Phys.* **1979**, *37*, 33.

(36) Anderson, P. W.; Weiss, P. R. *Rev. Mod. Phys.* **1953**, *25*, 269.